Nanoscale

Accepted Manuscript

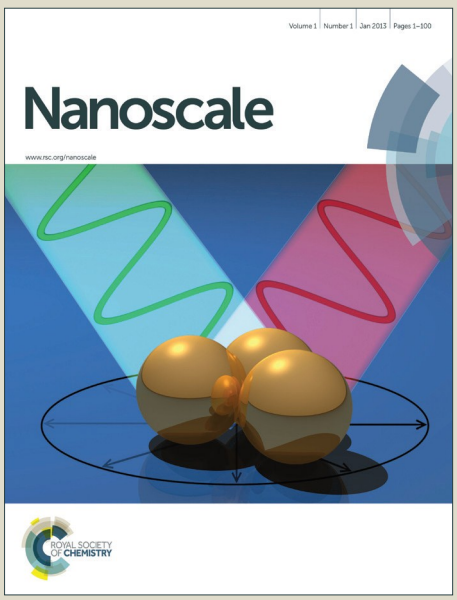

ROYAL SOCIETY OF CHEMISTRY

www.rsc.org/nanoscale

Journal Name

RSCPublishing

COMMUNICATION

Cylindrical nanostructured MoS_2 directly grown on CNT composites for lithium ion batteries

Cite this: DOI: 10.1039/x0xx00000x

HeeJoun Yoo[†3], Anand P. Tiwari[†1], JeongTaik Lee[2], Doyoung Kim[3], JongHyeok Park[2] and Hyoyoung Lee[*1]

Received (in XXX, XXX) Xth XXXXXXXXX 20XX,
Accepted Xth XXXXXXXXX 20XX

DOI: 10.1039/b000000x
www.rsc.org/

The direct attachment of MoS_2 to carbonaceous architecture materials remains a major challenge because of the non-intimate contact between carbonaceous materials and active MoS_2 material. In this study, we report a new unique synthesis method to produce a new type of hybrid nanostructure of MoS_2-CNTs composites. We developed a novel strategy for the synthesis of cylindrical MoS_2 directly grown on CNT composites without the use of any other additives, exhibiting super electrochemical performances as the anode material of lithium ion batteries via a microwave irradiation technique. We adopt a simple, step-by-step method: sulfur coating on CNTs and then reaction with a Mo source to synthesize hybrid cylindrical nanostructures of the MoS_2-CNT composite. X-ray diffraction, field emission scanning electron microscopy, and high-resolution transmission electron microscopy analyses demonstrated that the as-synthesized MoS_2-CNTs possessed a hybrid nanostructure in which MoS_2 sheets were well attached to the CNTs. The directly attached MoS_2 sheets on the CNTs showed superior electrochemical performance for anode materials of a lithium ion battery.

Rechargeable lithium ion batteries (LIBs), with high energy density and a long service life, have been widely used as portable electronic energy storage systems[1-3]. Recently, the demand for a portable energy source with higher capacity and power density has increased with the development of portable electronics and electric vehicles (EVs)[4]. The performance of LIBs is strongly dependent on the electrochemical properties of anode electrode materials[5,6]. Graphite has been commonly used for the anode electrode of LIB systems due to its flat potential profile versus lithium, high columbic efficiency, stable cycling performance and natural abundance. However, its relatively low specific capacity (372 mA h g^{-1}) and poor rate capability do not satisfy requirements for future portable electronics and EVs. Therefore, alternative superior anode materials are in demand for superior LIB systems [6].

Transition metal dichalcogenides (TMDs) are layered inorganic materials with an MX_2 crystal structure (M = Mo, Ti, V and W, X= S or Se) and that can intercalate and deintercalate alkali metal ions or foreign atoms into their interlayer structure. Therefore, TMDs can be considered as an anode electrode material for LIBs, and they show high theoretical capacity due to their conversion reaction with lithium ions[7-12]. Among TMD materials, molybdenum disulfide (MoS_2) has emerged as a promising anode electrode material[13-15]. Theoretically, MoS_2 sheets have a 1.8 times greater lithium storage capacity (670 mA h g^{-1}) than graphite, with the following conversion reaction:

$$MoS_2 + 4Li + 4e^- \rightarrow Mo + 2Li_2S$$

However, low rate capacity and bad cycling performance are still drawbacks of MoS_2[15-17]. MoS_2-carbon nanotube (CNT) composites show much better electrochemical performance due to synergy effect between them[18,19]. CNTs enhance the electric conductivity of MoS_2 and provide pores for lithium diffusion. In addition, CNT bundles prevent aggregation of MoS_2 during cycling and then maintain electric conductivity and a porous structure[20-22]. Various methods have been studied for the synthesis of MoS_2-CNTs including wet chemistry and a solvothermal reaction[18-22]. In MoS_2-CNT composites, MoS_2 should be attached to CNTs in order to produce a synergy effect between them[23]. However, MoS_2 is not closely attached to the CNTs, which continuously causes capacity fading during cycles and, as a result, leads to a lower specific capacitance[24-27]. There is no report of a method to directly attach MoS_2 layers on the CNT surface without the use of other additives.

Herein, we report a unique synthetic method of a cylindrical, nanostructured, directly grown MoS_2 layer on CNT composites and their LIB properties. We carefully design a simple step-by-step method to prepare the MoS_2 directly on CNT composites. Sulfur is coated on CNTs, and then the resulting sulfur-doped CNTs are reacted with the Mo source (Scheme 1). Sulfur is mixed with CNTs by grinding in a mortar with carbon disulfide (CS_2) solvent in which the sulfur is completely dissolved. Since sulfur has a strong interaction with the 6-membered carbon ring, sulfur-coated surfaces of CNTs are expected[28]. In the second step, the Mo-precursor solution is applied to the sulfur-coated CNT mixture. The resulting mixture is heated with microwaves

for few minutes under vacuum. The final morphology of the cylindrical MoS_2-CNT composites can be controlled by simply changing the solvent, which strongly affects the electrochemical performance of the MoS_2-CNT composite electrode for LIBs. The cylindrical nanostructured MoS_2 directly grown on CNT composites exhibit much better electrochemical performance for LIBs.

In 50 ml of CS_2 solvent, 200 mg of MWCNT and 200 mg of sulfur were mixed using a mortar to produce a sulfur-coated CNT composite (S-CNT). The resulting mixture was dried at RT in air. For preparation of the direct growth of MoS_2 on CNTs, 400 mg of molybdenum chloride ($MoCl_5$) was dissolved in ethanol, and the resulting solution was dropped into the S-CNT mixture and grinded with a mortar. The $MoCl_5$-S-CNT mixture was dried under vacuum at 60℃. To form MoS_2 on the surfaces of CNTs, the resulting mixture was treated with microwaves in an inert atmosphere at 700 W for 10 min to allow reaction with the incorporated sulfur and $MoCl_5$. Here, two different composites were synthesized with different conditions: MoS_2 directly grown on CNTs (MDGC-E) using ethanol as a $MoCl_5$ mixing solvent and a control sample of MoS_2 not directly grown on CNTs (MDGC-D) in a solvent of dichloromethane that can simultaneously dissolve sulfur and $MoCl_5$. The morphology, microstructure and chemical composition of the as-synthesized samples were investigated using a field-emission scanning electron microscope (FESEM) (JEOL JMM-740F), transmission electron microscope (TEM) (JEOL JEM-2100F), powder X-ray diffractometer (XRD) (Rigaku Ultima IV) Raman Spectroscopy, X-ray photospectroscopy (XPS) (ESCA 2000, VG Microtech) and thermogravimetric analysis (TGA).

2032 coin-type cells were used for the electrochemical measurements. The working electrode slurry was composed of MoS_2-CNT composites as an active material, carbon black (Super P) as a conductive additive, and poly (vinylidene fluoride) (PVdF) as a binder, at a weight ratio of 80:10:10 dissolved in N-methyl-2-pyrollidinone (NMP). The slurry was coated on copper foil as a current collector and dried under vacuum at 120 ℃ for 12 h. All 2032 coin-type cells were assembled in an Ar-filled glovebox. Lithium foil was used for both the counter and reference electrodes, and a polyethylene (PE) membrane (E16MMS, Tonen) was used as a separator. The 1M $LiPF_6$ used as an electrolyte was dissolved in a mixture of ethylene carbonate (EC) and diethyl carbonate (DEC, *v/v*, 1:1, Panax Etec Co., Ltd., Korea). The galvanostatic charge/discharge and cycling property measurements were performed using a multichannel battery test system (WonATech, Korea) at various current densities with a voltage range of 3–0.01V.

Scheme 1 reveals the schematic diagram for the synthesis of MoS_2 directly grown on CNTs composites via a microwave irradiation technique, as detailed in the Experimental Section. Mass production of high-quality, sulfur-coated CNT was obtained by mixing CNTs and sulfur in carbon disulfide. As the interaction between a sulfur molecule and the CNTs surface was strong due to their similar electronegativity values, the sulfur was well coated on CNTs *via* mixing. Sulfur is moderately sticky and insoluble in ethanol, which are present on the surfaces of CNTs while grinding with $MoCl_5$. The reaction between sulfur and

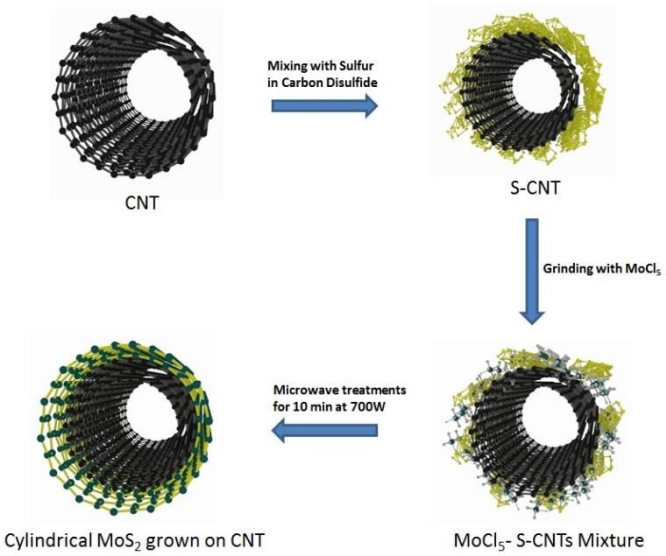

Scheme 1. Illustration of Cylindrical nanostructured MoS_2 directly grown on CNT

$MoCl_5$ occurs when the grinded mixture is treated with microwaves, and finally, MoS_2 is formed on the surfaces of the CNTs. The reaction to form MoS_2 can be describe as

$$2MoCl_5 + 4S \rightarrow 2MoS_2 + 5Cl_2$$

MoS_2-coated CNTs samples were first confirmed by X-ray diffraction (XRD). The XRD patterns of sulfur- and MoS_2-coated CNTs samples, S-CNTs, MDGC-D, and MDGC-E, are shown in Figures 1 (a), (b) and (c), respectively.

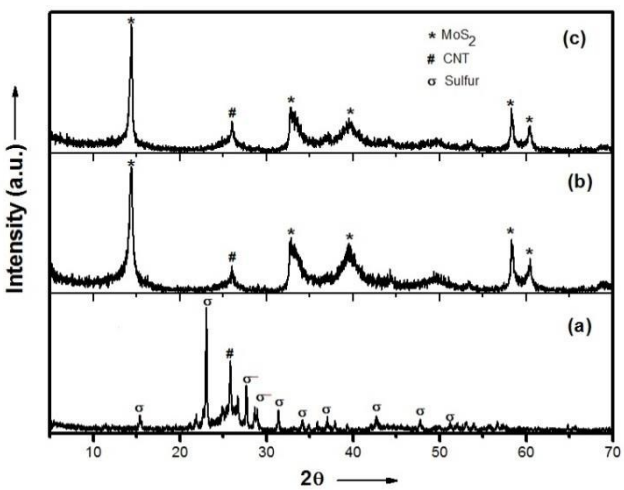

Figure 1 XRD patterns of (a) S-CNTs, (b) MDGC-D and (c) MDGC-E samples.

The XRD patterns in Figures 1(b) and 1(c) are indexed as hexagonal 2H-MoS_2 (JCPDS 6-97). The single strong (002) reflection at $2\Theta = 14.2^0$, corresponding to a d-spacing of 0.615 nm, reveals a well-stacked layered structure of MoS_2 for both MDGC-D and MDGC-E. Moreover, the diffraction peaks of the MDGC-D and MDGC-E samples at $2\Theta = 33.5^0$, 39.6^0, and 59.1^0

correspond to the (100), (103), and (110) planes of MoS_2, respectively. This shows that microwave treatment was sufficient for obtaining good crystallinity of MoS_2. Surprisingly, sulfur peaks are not present in the samples shown in Figures 1(b) and 1(c), whereas they are present in the sulfur-coated CNT sample displayed in Figure 1(a), revealing that the microwave treatment for 10 min is sufficient to form well-stacked MoS_2 layers from $MoCl_5$.

To determine the chemical composition of MoS_2 coated CNT composites MDGC-E and MDGC-D, X-ray photospectroscopy (XPS) measurements were carried out in the region of 0 ~1100 eV. Supplementary Figures S1(a) and S1(b) show that the sample contains the C, Mo and S elements. The calculated atomic ratio of Mo to S element is 1 to 2.14 and 1 to 2.20 for MDGC-E and MDGC-D samples, approaching the theoretical value of MoS_2. The high-resolution of C1s can be seen apart from the "C = C" bond.

To confirm the coating of MoS_2 on the CNT surfaces the Raman spectroscopy were carried out using an excitation wavelength of 514 nm. Supplementary Figures S2(c) and S2(d) show the Raman spectra of MoS_2 coated CNT composites MDGC-D and MDGC-E. It can be clearly seen that there are two peaks at 382 cm^{-1} and 405 cm^{-1} correspond to E_{2g} and A_{1g} peaks of MoS_2 which implies that MoS_2 has well layered structure on the surface of CNT.

The microstructures of as-prepared MoS_2 directly grown on CNTs samples were examined in detail using TEM and HRTEM. The TEM and HRTEM images of MDGC-E are shown in Figures 2 (a) and (b), respectively. As shown in Figures 2(a) and (b), MoS_2 sheets were well supported on CNTs with $d_{(002)}$ = 0.61 nm, which corroborates the XRD pattern of MDGC-E (Figure 1(c)). As shown in the HRTEM (Figure 2 (b), Supplementary information Figure S4 (a)) images, there were at least 4–8 layers of MoS_2 bonded by van der Waals interactions. Figures 2(c) and (d) show the TEM and HRTEM images of the MDGC-D sample, demonstrating the absence of the well-layered structure of the MoS_2 sheets. Furthermore, there was also residual sulfur in the MDGC-D sample (Figure 2 (d)). The MoS_2 sheets were not well coated on the CNTs, as shown in Figures 2 (c) and (d). Figure 2

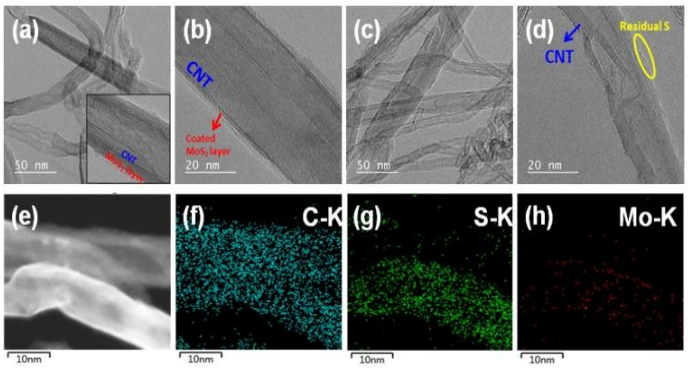

Figure 2 TEM and HRTEM images of (a, b, e) MDGC-E and (c, d) MDGC-D; (f – h) the elemental mapping image of MDGC-E

(e) is a dark field TEM image of the MDGC-E sample. The elemental composition of the MDGC-E sample was determined by elemental mapping using energy dispersive X-ray photospectroscopy (EDX), as shown in Figures 2 (f), (g), and (h).

MoS_2 contains mostly Mo and S with only a trace presence of C. The strong presence of C in the sample is clearly a contribution from the CNTs. The amount of MoS_2 in MDGC-E sample is calculated by TGA. It is found that MDGC-E sample contains 14.02 wt% of MoS_2 and 85.98 wt% of C (Supplementary Figure S3).

Figures 3 (a), (b), (c) and (d) show the SEM images of CNTs, S-CNTs, MDGC-E, and MDGC-D samples, respectively. As shown in Figures 3 (a) and (b), sulfur was uniformly coated on the CNT surfaces. The MoS_2 sheets were also well coated on the CNTs surfaces, as shown in Figure 3 (c). Additionally, the MDGC-E sample also contained sphere-like particles. It is reasonable to assume that the layered structure of MoS_2 would naturally give rise to a flake-like morphology. Alternatively, MoS_2 sheets were not grown on the surfaces of CNTs of the MDGC-D sample, as shown in Figure 3 (d), which agrees with the TEM analysis in Figure 2(d). Furthermore, MoS_2 particles of the MDGC-D sample shown in the inset of Figure 3(d) were agglomerated through separation with CNTs, which is different from the MDGC-E sample displayed in Figure 3(c).

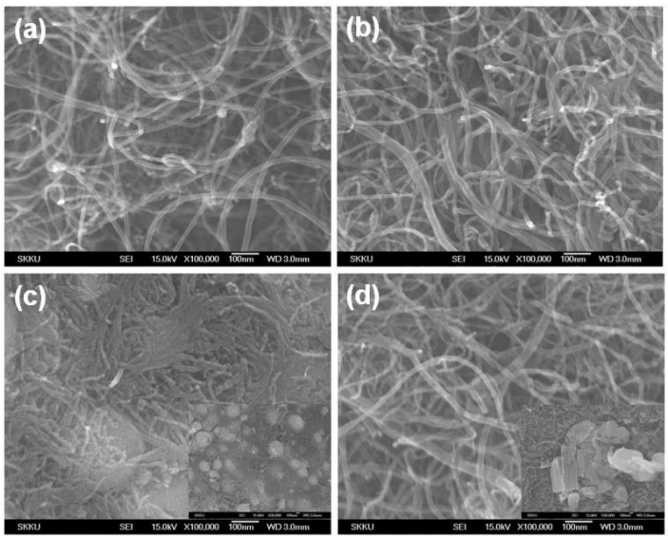

Figure 3 SEM images of (a) CNTs, (b) S-CNTs, (c) MDGC-E and (d) MDGC-D.

The electrochemical performances were investigated by cyclic voltammetry (CV) and galvanostatic charging-discharging cycling. Figure 4(a) voltammograms of the first three cycles of MDGC-E. The as-synthesized MDGC-E sample shows two reduction peaks at 0.9 and 0.4 V in the first cathodic sweep, as shown in Figure 4(a). The peak at 0.4 V is attributed to the conversion reaction process[29,30].

$$MoS_2 + 4Li + 4e^- \rightarrow Mo + 2Li_2S$$

However the peak at 0.9 V can be attributed to the coordination of Mo by six S atoms (MoS_6), which changes from trigonal prisms to octahedral in the MoS_2 structure along with the intercalation of lithium in MoS_2. These reduction peaks disappear from the second cycle because of the decomposition of MoSx

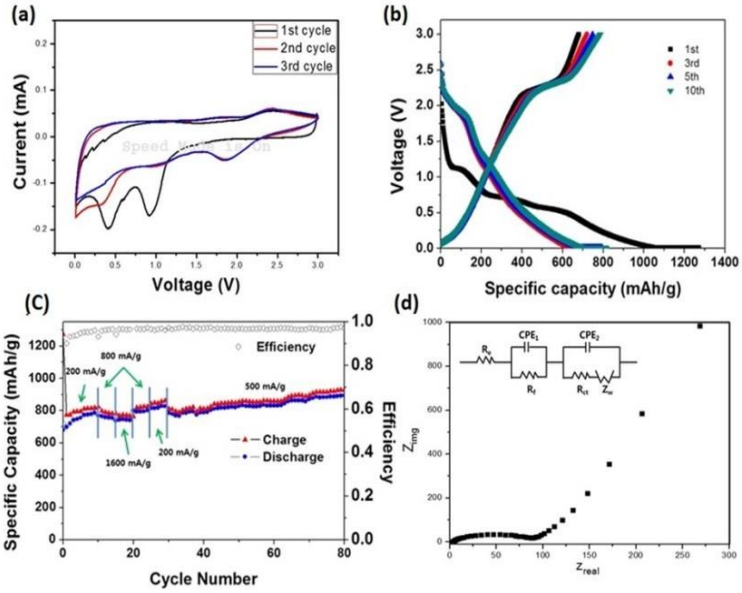

Figure 4 (a) Galvanostatic charge and discharge curves (b) Cycling and rate performances (C) First three cyclic voltammograms and (d) Nyquist plot of MDGC-E

into Mo nanoparticles embedded in the Li_2S matrix through the conversion reaction which agrees well with previous reported MoS_2/carbon composites prepare by hydrothermal rout[31-34]. This is important evidence for the MoS_2 coating structure on CNT. Due to the close coating structure between the MoS_2 layer and CNT, the conversion reaction of MoSx during the reduction potential is facilitated.

Figures 4(b) shows discharge-charge profiles of the 1st, 3rd, 5th, and 10th cycles of the MDGC-E sample at a current density of 50 mA/g. Figure 4(b) exhibits three potential plateaus at 1.20 V, 0.7 V, and below 0.2 V for the MDGC-E electrodes in the first discharge process. The plateau at 1.20 V confirms the formation of Li_xMoS_2, and the plateau at 0.7 V suggests the conversion reaction in which MoS_2 decomposes into Mo particles embedded in a Li_2S matrix[35]. However, the plateau at the potential below 0.2 V demonstrates lithium deintercalation from CNTs[36]. The slope potential beyond 0.7 V indicates the formation of a gel-like polymeric layer from electrochemical-driven, electrolyte degradation. Moreover, the 3rd, 5th, and 10th discharge curves of the MDGC-E electrode show plateaus at 1.9 V, 1.2 V, and below 0.2 V, which is consistent with previous reports[24,25]. The charge process of the MDGC-E electrode displays two conspicuous potential plateaus at 0.20 V and 2.25 V due to the high crystallinity of MoS_2 and lithium intercalation in the CNTs. Alternatively, potential plateaus at 1.70 V, 0.7 V and below 0.2 V in the first discharge process of the MDGC-D sample electrode were observed, as shown in Supplementary Figure S4. However in the 3rd and 5th discharge processes of the MDGC-D electrode, potential plateaus at 0.70 V are barely visible, and neither potential plateau at 1.70 V or 0.70 V is observable in the 10th cycle of the MDGC-D sample (Supplementary Figure S5), which is quite different from the MDGC-E sample. This behavior of the MDGC-D electrode sample was due to the agglomeration of MoS_2 by CNTs (Figure 3(d)).

Figure 4(b) illustrates that the initial discharge capacity of the MDGC-E electrode was 1,280 mAh/g, while the initial reversible charge capacity was 790 mAh/g. The irreversibility in the first cycles is due to the formation of a solid electrolyte interface (SEI) film, decomposition of the electrolyte, and reduction of oxygen-containing groups. The specific capacity of the MDGC-E electrode was much greater than the theoretical capacity of bulk MoS_2 (167 mAh/g)[37]. Moreover, the initial discharge and charge capacities of the MDGC-D electrode were 1680 and 920 mAh/g, respectively (Supplementary Figure S5). Figure 4(c) shows the cyclic stability of the MDGC-E electrode at different current densities. The reversible charge and discharge capacities of the MDGC-E electrode increase from 822 and 984 mAh/g, respectively, after 10 cycles at a constant current density of 200 mA/g with 95.8% columbic efficiency. Surprisingly, when the current densities increase from 200 to 800 and 1600 mA/g, the MDGC-E electrode shows good capacity retention as the specific discharge capacities change from 984 to 894 and 670 mAh/g, respectively. Even when the current density changed to 1600 mA/g, the capacity was maintained at 670 mAh/g. Additionally, when the current density returned to 200 mA/g, the specific capacity of the sample returned to original values, illustrating that the MDGC-E electrode exhibited good high-rate performances. The MDGC-E electrode maintains its charge and discharge capacities at a current density 500 mA/g up to 80 cycles.

Electrochemical impedance spectrometry (EIS) measurements were performed after 10 cycles in order to better understand the electrochemical performances of MoS_2 coated CNT composite electrode. Figure 4(c) shows the Nyquist plots of the MDGC-E electrodes. The equivalent circuit model for the impedance response is inserted in Figure 4(c) where Re represents the internal resistance, Rf and CPE1 are the resistance and constant phase element of the SEI, respectively, Rct and CPE2 are the charge-transfer resistance and constant phase element of the electrode/electrolyte interface, respectively, and Zw is the Warburg impedance corresponding to the lithium diffusion process[31]. The high frequency semicircle in Figure 4(c) corresponds to the resistance, Rf, and CPE1 of the SEI film. Meanwhile, the medium frequency semicircle can be attributed to the charge-transfer resistance, Rct, and CPE2 of the electrode/electrolyte interface whereas the inclined line in the low frequency region corresponds to lithium diffusion processes. The Rf and Rct values were obtained by modeling ac impedance spectra based on a modified equivalent circuit[38]. The Rf and Rct values of the MDGC-E electrode are 14.69 Ω and 91.30 Ω, respectively. The Rf and Rct values of the MDGC-E electrode are lower than those of previously reported MoS_2 electrodes[39,40], which confirms that the CNT preserve the improved conductivity and enhance the rapid electron transport during the Li ion insertion/extraction reaction.

It is assumed that the high specific capacity, high rate capability and rapid electron transport of the MDGC-E electrode can be ultimately attributed to the expanded interlayer distances between MoS_2 directly grown on the CNT sheets, which can intercalate

more Li^+ ions between MoS_2–CNTs. Additionally, the high cyclic stability is due to the lack of aggregation of MoS_2 itself as a result of the direct growth of MoS_2 on the CNT sheets. This type of cylindrical and 3D-nanostructured architecture provides a high contact area and a largely expanded interlayer distance, which play an important role in absorbing more Li^+. In contrast, the MDGC-D electrode that does not have MoS_2 layers on the surfaces of CNTs as a result of the agglomeration of MoS_2 particles through separation with CNTs, as shown in Figure 3(d), shows poor cycling ability and poor rate capability (Supporting Information Figure S6).

In summary, we developed a novel strategy for the synthesis of cylindrical MoS_2 directly grown on CNT composites without the use of any other additives. The characterization of the 3D micro and nanostructures by XRD, TEM, and SEM indicates that the MoS_2 sheets were well grown on the CNT surface, especially for the MDGC-E sample. Electrochemical evaluations showed that the MoS_2 directly grown on the CNTs electrodes had greater specific capacity, excellent cycling property, and good rate capability. The excellent electrochemical performance as anode materials for lithium ion batteries can be attributed to the synergistic effects of cylindrical, 3D nanostructured MoS_2 directly grown on CNTs composites. This performance is illustrated by maintenance of porosity for Li^+ ions, prevention of aggregation by direct growth of MoS_2 on CNTs, and production of high conductivity CNTs for an insulating MoS_2 used as anode materials. The cylindrical, 3D nanostructured MoS_2 directly grown on CNT composites can be applied as very versatile anode material for Li-ion batteries.

This work was supported by the Creative Research Initiatives funded by the Ministry of Science, ICT and Future Planning (No.2006-0050684) and partially by ISTK (Grant B551179-13-01-01)

Notes and references

1 *Department of Chemistry, Sungkyunkwan University, 2066 Seoburo, Jangan-Gu, Suwon, Gyeonggi-Do 440-746, South Korea. Email: hyoyoung@skku.edu; Fax: (+) 82-31-299-5934; Tel: (+) 82-31-299-4566;*
2 *School of Chemical Engineering, Sungkyunkwan University, Suwon 440-746, Republic of Korea*
3 *Department of Energy Science, Sungkyunkwan University, 2066 Seoburo, Jangan-gu, Suwon, Gyeonggi-do 440-746, Republic of Korea*
† Equally contributed
Electronic supplementary information (ESI) available

1 V. Etacheri, R. Marom, R. Elazari, G. Salitra, D. Aurbach, *Energy Environ. Sci.*, 2011, 4, 3243- 3262.
2 M. Armand, J. M. Tarascon, *Nature*, 2008, 451, 652-657.
3 B. Dunn, H. Kamath, J. M. Tarascon, *Science*, 2011, 334, 928-934.
4 J. Wen, Y. Yu, C. Chen, *Mater. Express*, 2012, 2, 197-212.
5 N.S. Choi, Z. Chen, S. A. Freunberger, X. Ji, Y. K. Sun, K. Amine, G. Yushin, L. F. Nazar, J. Cho, P. G. Bruce, *Angew. Chem.*, 2012, 51, 9994-10024.
6 M. Winter, R. J. Brodd, *Chem. Rev*., 2004, 104, 4245-4269.
7 N. F. Zhang, X. H. Bu, P. Y. Feng, *Nature* 2003, 426, 428-432.
8 M. S. Whittingham, *Science* 1976, 192, 1126-1127.
9 E. Benavente, M.A. Santa Ana, F. Mendizabal, G. Gonzalez, *Coord. Chem. Rev*., 2002, 224, 87-109.
10 H. S. S. R. Matte, A. Gomathi, A. K. Manna, D. J. Late, R. Datta, S. K. Pati, C. N. R. Rao, *Angew. Chem.*, 2010, 49, 4059-4062.
11 S. J. Ding, D. Y. Zhang, J. S. Chen, X. W. Lou, *Nanoscale*, 2012, 4, 95-98.
12 G. D. Du, Z. P. Guo, S. Q. Wang, R. Zeng, Z. X. Chen, H. K. Liu, *Chem. Commun*., 2009, 46, 1106-1108.
13 T. Stephenson, Z. Li, B. Olsen, D. Mitlin, *Energy Environ. Sci.*, 2014, 7, 209-231.
14 X. L. Li, Y. D. Li, *J. Phys. Chem. B*, 2004, 108, 13893-13900.
15 X. P. Fang, X. Q. Yu, S. F. Liao, Y. F. Shi, Y. S. Hu, Z. X. Wang, G. D. Stucky, L. Q. Chen, *Microporous Mesoporous Mater.*, 2012, 151, 418-423.
16 H. Liu, D. Su, R. Zhou, B. Sun, G. Wang, S. Z. Qiao, *Adv. Energy Mater.*, 2012, 2, 970-975.
17 H. Hwang, H. Kim, J. Cho, *Nano Lett.*, 2011, 11, 4826-4830.
18 K. Bindumadhavan, S. K. Srivastava and S. Mahanty, *Chem. Commun.*, 2013, 49, 1823-1825.
19 Y. Shi, Y. Wang, J. Wong, A. Y. S. Tan, C. L. Hsu, L. J. Li, Y. C. Lu, H. Y. Yang, *Scientific Report*, 2013, 3, 2169-2176.
20 S. Wang, X. Jiang, H. Zheng, H. Wu, S. Kim, C. Feng, *Nanoscience and Nanotechnology Letters*, 2012, 4, 378-383.
21 L. Ma,W. X. Chen, Z. Xu, J. Xia, X, Li, *Nanotechnology*, 2006, 17,571-574.
22 V.O. Koroteev, L.G. Bulusheva, I. P. Asanov, E.V. Shlyakhova, D.V. Vyalikh, A.V. Okotrub, *The Journal of Physical Chemistry C*, 2011, 115, 21199-21204.
23 Y. Gong, S. Yang, Z. Liu, L. Ma, R. Vajtai, P. M. Ajayan, *Adv. Mater.* 2013, 25, 3979-3984.
24 K. Chang , W. X. Chen , *J. Mater. Chem.* 2011, 21, 17175-17184.
25 Q. Zhang, K. Yu, B. Zhao, Y. Wang, C. Song, S. Li, H. Yin, Z. Zhang, Z. Zhu, RSC Advances, 2014,
26 X. Cao, Y. Shi, W. Shi, X. Rui, Q. Yan, J. Kong, H. Zhang, *Small*, 2013, 9, 3433-3438.
27 G. Huang, T. Chen, W. Chen, Z. Wang, K. Chang, L. Ma, F. Huang, D. Chen, J. Y. Lee, *Small* 2013, 9, 3693-3703.
28 T. Lin, Y. Tang, Y. Wang, H. Bi, Z. Liu, F. Huang, X. Xie, M. Jiang, *Energy Environ. Sci.*, 2013, 4, 1283-1290.
29 K. Chang, W. Chen, L. Ma, H. Li, H. Li, F. Huang, Z. Xu, Q. Zhang, J. Y. Lee, *J. Mater. Chem*., 2011, 21, 6251-6257.
30 G. X. Wang, S. Bewlay, J. Yao, H. K. Liu, S. K. Dou, *Electrochem. Solid-State Lett.* 2004, 7, A321-A323.
31 K. Chang, W. Chen, *ACS Nano*, 2011, 5, 4720-4728.
32 Z. Wang, T. Chen, W. Chen, K. Chang, L. Ma, G. Huang, D. Chen, J. Y. Lee, *J. Mater. Chem. A*, 2013, 1, 2202-2210.
33 C. Zhu, X. Mu, P. A Aken, Y. Yu, J. Maier, *Angew. Chem.*, 2014, 53, 2152 –2156.

34 G. Huang, T. Chen, W. Chen, Z. Wang, K. Chang , L. Ma, F. Huang, D. Chen, J. Lee, *Small*, 2013, 9, No. 21, 3693–3703.
35 R. Dominko, D. Arcon, A. Mrzel, A. Zorko, P. Cevc, P. Venturini, M. Gaberscek, M. Remskar, D. Mihailovic, *Adv. Mater.*, 2002, 14, 1531-1533.
36 M. Yoshio, H. Wang, K. Fukuda, Y. Hara, Y. Adachic, *J. Electrochemical Society*, 2000, 147, 1245-1250.
37 J. Xiao, D. Choi, L. Cosimbescu, P. Koech, J. Liu, J. P. Lemmon, *Chem. Mater.*, 2010, 22, 4522-4524.
38 S. B. Yang, X. L. Feng, L. J. Zhi, Q. A. Cao, J. Maier, K. Mullen, Adv. Mater. 2010, 22, 838.
39 Y. Hou, J. Li, Z. Wen, S. Cui, C. Yuann, J. Chenn, *Nano Energy*, 2014 8, 157–164.
40 X. B. Chen, J. H. He, D. Srivastava, J. Li, Appl. Phys. Lett., 2012, 100, 263901.

Table of Content (TOC)

An effective approaches is developed to synthesize a cylindrical, 3D nanostructured, MoS_2 on CNTs composites for high-performance Li-ion batteries.